

DETAILED THEORETICAL PREDICTIONS FOR THE OUTSKIRTS OF DARK MATTER HALOS

JUAN E. BETANCORT-RIJO^{1,2}, MIGUEL A. SANCHEZ-CONDE³, FRANCISCO PRADA³ AND SANTIAGO G. PATIRI¹

¹ Instituto de Astrofísica de Canarias, Vía Láctea s/n, La Laguna, Tenerife, E38200, Spain

² Facultad de Física, Universidad de La Laguna, Astrofísico Francisco Sanchez, s/n, La Laguna Tenerife, E38200, Spain and

³ Instituto de Astrofísica de Andalucía (CSIC), E18008, Granada, Spain

Draft version February 5, 2008

ABSTRACT

In the present work we describe the formalism necessary to derive the properties of dark matter halos beyond two virial radius using the spherical collapse model (without shell crossing), and provide the framework for the theoretical prediction presented in Prada et al. (2005). We show in detail how to obtain within this model the probability distribution for the spherically-averaged enclosed density at any radii $P(\delta, r)$. Using this probability distribution, we compute the most probable and mean density profiles, which turns out to differ considerably from each other. We also show how to obtain the typical profile, as well as the probability distribution and mean profile for the spherically averaged radial velocity. Three probability distributions are obtained: a first one is derived using a simple assumption, that is, if Q is the virial radius in Lagrangian coordinates, then the enclosed linear contrast $\delta_l(q)$ must satisfy the condition that $\delta_l(q = Q) = \delta_{vir}$, where δ_{vir} is the linear density contrast within the virial radius R_{vir} at the moment of virialization. Then we introduce an additional constraint to obtain a more accurate $P(\delta, r)$ which reproduces to a higher degree of precision the distribution of the spherically averaged enclosed density found in the simulations. This new constraint is that, for a given $q > Q$, $\delta_l(q) < \delta_{vir}$. A third probability distribution, the most accurate, is obtained imposing the strongest constraint that $\delta_l(q) < \delta_{vir} \quad \forall q > Q$, which means that there are no radii larger than R_{vir} where the density contrast is larger than that used to define the virial radius. Finally, we compare our theoretical predictions for the mean density and mean velocity profiles with the results found in the simulations.

Subject headings: cosmology:theory — dark matter — large-scale structure of universe — methods:analytical

1. INTRODUCTION

The study of the density profile of cold dark matter halos beyond the virial radius is a subject of considerable relevance. From an observational point of view, knowledge of the shape of the density profile far beyond the virial radius is essential for an appropriate interpretation of gravitational lensing phenomena (e.g. Smith et al. 2001; Guzik & Seljak 2002; Hoekstra et al. 2004; Sheldon et al. 2004), the pattern of Lyman alpha absorption around virialized systems (e.g. Barkana 2004; Bajtlik, Duncan & Ostriker 1988) as well as the motion of satellite galaxies as a test for dark matter distribution at large radii (Zaritsky & White 1994, Zaritsky et al. 1997; Prada et al. 2003, Brainerd 2004; Conroy et al. 2004). From the theoretical point of view, the study of the properties of dark matter halos at several virial radius in cosmological simulations provides an excellent benchmark for developing and testing the basic theoretical framework which will be decisive for a full understanding of the physical origin and formation of the Λ CDM halos.

Understanding halo properties involves a set of theoretical considerations. First, we have the issue of choosing the correct initial density profile. Also, there is the question of which processes are relevant to the gravitational evolution of the initial profile: is only the spherical collapse what matters or is triaxiality important? up to which radius can we use the standard spherical collapse model without shell crossing? are highly asymmetrical processes, like merging, relevant? In order to answer these questions it is very convenient to focus first on those properties of the halos which involve the fewest theoretical uncertainties.

The dark matter density profiles at several virial radius

are particularly suitable to check whether the spherical collapse model can provide accurate predictions (see Prada et al. 2005). In fact, it has been shown that the spherical collapse model reproduces very well the relationship between the small values of the spherically-averaged enclosed density at those large distances and the radial velocity (Lilje et al. 1986).

We define the spherically-averaged enclosed density as:

$$\frac{\rho(< r)}{< \rho_m >} = 1 + \delta$$

where δ is the enclosed density contrast and $< \rho_m >$ the average matter density in the Universe. We can also define the spherically-averaged local density as:

$$\frac{\rho(r)}{< \rho_m >} = 1 + \delta'$$

where δ' is the density contrast in a narrow shell of radius r . We can then obtain the density contrast δ' from the enclosed density contrast δ using the relation:

$$\delta'(r) = \frac{1}{3r^2} \frac{d}{dr}(r^3 \delta(r)).$$

Despite to all the effort done to understand the central dense regions of the dark matter halos in cosmological simulations, not much attention has been devoted to the study of the regions beyond the formal virial radius, i.e. the radius within which the spherically-averaged enclosed density is equal to some specific value. The main goal of the work presented in this paper is focused on the outskirts of the dark matter halos, where the correct evolution of the spherically-averaged enclosed density profiles can essentially be obtained using the standard (without shell crossing) spherical collapse model.

This model, first developed by Gunn & Gott (1972) and Gunn (1977), describes the collision-less collapse of a spherical perturbation in an expanding background. They introduced for the first time the cosmological expansion and the role of adiabatic invariance in the formation of individual objects. Later, Fillmore & Goldreich (1984) found analytical predictions for the density of collapsed objects seeded by scale-free primordial perturbations in a flat universe. Hoffman & Shaham (1985) generalized these solutions to realistic initial conditions in flat and open Friedmann models. Some studies have been done to include more realistic dynamics of the growth process (e.g. Padmanabhan 1996; Avila-Reese, Firmani & Hernández 1998; Lokas 2000; Subramanian, Cen & Ostriker 2000).

There are plenty of works in the literature using the spherical collapse model to predict the density profiles of dark matter halos mainly focused on explaining their central regions. For example Bertschinger (1985) used the spherical collapse with shell crossing to obtain the density profiles resulting from initial power law density profiles. Lokas & Hoffman (2000) considered more general initial profiles. The effect of non-radial motions has also been widely treated (see Ryden & Gunn 1987; Gurevich & Zybin 1988; Avila-Reese et al. 1998; White & Zaritsky 1992; Sikivie et al. 1997; Nusser 2001; Hiotelis 2001). Some of these authors have used arbitrary initial profiles, while others have assumed the mean initial profile around density maxima (Bardeen et al. 1986, BBKS). In all these works angular momentum is introduced by hand, although more recently it has been done in a more natural way (Nusser 2001; Ascasibar et al. 2004). Concerning to the outer parts of the dark matter halos, only Barkana (2004) has adopted an appropriate initial profile, but only for a restricted type of density profile (the typical profile). The more recent work by Prada et al. (2005) have obtained predictions for the mean and most probable density profiles and have provided a detailed comparison with cosmological simulations.

A proper understanding of the physics of dark matter halos involves predicting correctly not only the mean halo density profile for any given mass but also the whole probability distribution for the enclosed density contrast at any given radii, $P(\delta, r)$. A first attempt to determine it can be found in Prada et al. (2005), where it has been shown to be generally in good agreement with the cosmological simulations. Nevertheless, this probability distribution shows, at any radius, a longer tail for large values of δ , as compared to that from simulations at any radius. In this paper we present a more accurate prediction for the probability distribution $P(\delta, r)$ that constitutes the main new result of this work. We also give in detail the theoretical background of the predictions presented in Prada et al. (2005). The agreement of our new predictions with the simulations is excellent even in the tail of the distribution. Furthermore, we also compute the radial velocity probability distribution and the mean radial velocity profile.

The work is organized as follows. In section 2 we present our theoretical framework and obtain the typical density profile of dark matter halos. In section 3 we show in detail how to obtain the probability distribution for the spherically-averaged enclosed density contrast at a given radii, $P(\delta, r)$, presented in Prada et al. (2005). The most probable and mean profiles are derived. In section 4, we compute the probability distribution and mean profile for the spherically averaged radial velocity. In section 5, we obtain more accurate probability distributions than that used in the previous sections, and compare again

with that found in the simulations. Final remarks are given in section 6.

2. THE TYPICAL DENSITY PROFILE OF DARK MATTER HALOS

The present spherically-averaged enclosed density profiles attains a density contrast value of Δ_{vir} at certain radius, the so called virial radius. At larger radii the density contrast must be, by definition, smaller than Δ_{vir} , otherwise the virial radius would be larger than its nominal value.

We shall now make some comments on the values of Δ_{vir} and δ_{vir} that we use: although at several virial radius the spherically-averaged enclosed linear and actual densities are related by the spherical collapse model, the same does not apply within the virial radius. The spherically-averaged enclosed density contrast within one virial radius, Δ_{vir} , and the corresponding enclosed linear density contrast, δ_{vir} , are not related as homologous quantities at larger radii, because at one virial radius shell crossing has already becomes important. Consequently, the value of δ_{vir} corresponding to $\Delta_{vir}=340$ (the value we adopted to define the virial radius) is somewhat uncertain. As a result of work still in progress we will be able to provide the precise values for δ_{vir} and determine its possible small dependence on mass. Here we use for all masses $\delta_{vir}=1.9$, a value that leads to very good results and that may be inferred from the fact that when $\Delta_{vir}=180$, δ_{vir} seems to be close to 1.68 for all cosmologies (Jenkins et al. 2001).

It must be noted that for all our predictions it is irrelevant whether the value of Δ_{vir} that we use actually corresponds to the virial density contrast or not. By virial density contrast is usually meant the enclosed density contrast within the largest radii so that we have statistical equilibrium. The precise value of Δ_{vir} corresponding to this definition is still problematic but, to our purposes, it can be chosen freely to define a conventional "virial radius". Since we have used numerical simulations with Δ_{vir} equal to 340, we will take the same value by default in all the calculations.

Let $\delta_i(q, i)$ be a realization of the spherically-averaged initial enclosed density profile around a protohalo (with a given present virial radius, R) linearly extrapolated to the present, where q is the lagrangian distance from the center of the halo to the given point and i is an index running over realizations. Any realization of the initial profile may be transformed using the standard spherical collapse model (without shell-crossing). We can use the relationship between the linear value of the density contrast within a sphere, δ_i , and the actual density contrast within that sphere, δ , for the concordant cosmology (Sheth and Tormen (2002)):

$$\delta_i(\delta) = \frac{1.676}{1.68647} \left[1.68647 - \frac{1.35}{(1+\delta)^{2/3}} - \frac{1.12431}{(1+\delta)^{1/2}} + \frac{0.78785}{(1+\delta)^{0.58661}} \right] \quad (1)$$

or, rather its inverse function $\delta(\delta_i)$ (Patiri et al.(2004) expression (4)):

$$\delta(\delta_i) = 0.993 \left[(1 - 0.607(\delta_i - 6.5 \times 10^{-3}(1 - \theta(\delta_i)) + \theta(\delta_i - 1.55))\delta_i^2)^{-1.66} - 1 \right] \quad (2)$$

being θ the step function:

$$\theta(x) = \begin{cases} 1 & \text{if } x > 0 \\ 0 & \text{if } x \leq 0 \end{cases}$$

Transforming for every shell δ_i and q into δ and r (the Eulerian radius of the shell) we may obtain, in parametric form, the initial profile $\delta_i(q, i)$ spherically evolved, $\delta(r, i)$.

$$\delta(r, i) = \delta(\delta_l(q, i)); \quad r = [1 + \delta(\delta_l(q, i))]^{-1/3} q \quad (3)$$

This two equations gives $\delta(r, i)$ implicitly with q as parameter.

We must now eliminate all linear profiles leading to present profiles which attains an enclosed density contrast larger than (or equal to) Δ_{vir} at a radii larger than the nominal virial radius. The ensemble of remaining halos allow us to obtain the predictions of the standard spherical collapse model for any statistics. For example, we shall obtain the predictions for the mean profile:

$$\bar{\delta}(r) \equiv \langle \delta(r, j) \rangle_j$$

That is, the average over all remaining halos (j runs over these halos). We shall also consider the most probable profile, $\delta_p(r)$, that is, the profile that associates with every value of r the δ value with the largest probability density.

The procedure described above to obtain the spherical model predictions (i.e. realizations of the linear profile evolved with expression (3)) serve mostly to the purpose of clarifying the meaning of those predictions and we only use it as a test to the analytical expressions. In practise, we shall use another procedure to obtain directly $\bar{\delta}(r)$, $\delta_p(r)$ and, in fact, the whole probability distribution for the value of δ at a given value of r , $P(\delta, r)$.

Before dealing with the detailed predictions just mentioned we consider a simpler prediction which shall help clarifying the rest of the work, and which is related to previous approaches (Barkana 2004).

Consider the ensemble of all halos, $\delta(r, j)$, attaining a δ value equal to Δ_{vir} at a virial radius and smaller values for larger radii. If we transform back these profile to their linear counterpart, we obtain the ensemble $\delta_l(q, j)$. Let us now take the average over this ensemble (now for a fixed value of q):

$$\bar{\delta}(q) \equiv \langle \delta(q, j) \rangle_j$$

Evolving this profile by means of the spherical collapse model we obtain a profile which we call typical profile and represent by $\delta_l(r)$, that is, this profile is simply the mean profile in the initial conditions spherically evolved.

Note that the typical density profile is defined because of its simplicity and not because it constitutes a prediction for any specific statistics of the actual halos. Nevertheless, it should not be very different from the most probable profile. Later we will study how these two profiles differ from each other. This profile definition is the same as that used by Barkana (2004), but we use a different approximation to derive it.

To obtain the mean linear density profile $\bar{\delta}_l(q)$ subject to the condition that in the present enclosed density profile the virialization density contrast, Δ_{vir} , is not attained beyond the virial radius, Barkana used barrier penetration results. He obtained the probability distribution for $\delta_l(q)$ given the conditions:

$$\delta_l(Q) = \delta_{vir}; \quad \delta_l(q) < \delta_{vir} \quad \forall q > Q$$

$$Q \equiv R_{vir}(1 + \Delta_{vir})^{1/3}$$

where R_{vir} is the virial radius (Q the corresponding Lagrangian radius), and δ_{vir} is the linear counterpart of Δ_{vir} . Then, by averaging over all δ_l values smaller than δ_{vir} , he obtained the mean linear profile, $\bar{\delta}_l(q)$, with those conditions. However, he had to make some simplifications, the most relevant one is that he used a sharp filter in k -space, rather than

the top hat filter in ordinary space which is the natural one in this context.

In our approach we first obtain the probability for $\delta_l(q)$ only with the condition $\delta_l(Q) = \delta_{vir}$:

$$P(\delta_l, q) \equiv P(\delta_l(q) | \delta_l(Q) = \delta_{vir}) = \frac{\exp\left(-\frac{1}{2} \frac{(\delta_l(q) - \frac{\sigma_{12}}{\sigma_1} \delta_{vir})^2}{g}\right)}{\sqrt{2\pi} g^{1/2}} \quad (4)$$

where

$$g(q) \equiv \left(\sigma_2^2 - \frac{\sigma_{12}^2(q)}{\sigma_1^2} \right)$$

$$\sigma_1 \equiv \sigma(Q); \quad \sigma_2 \equiv \sigma(q)$$

$$(\sigma(x))^2 = \frac{1}{2\pi^2} \int_0^\infty |\delta_k|^2 W_T^2(xk) k^2 dk$$

$$\sigma_{12} = \sigma_{12}(q) = \frac{1}{2\pi^2} \int_0^\infty |\delta_k|^2 W_T(qk) W_T(Qk) k^2 dk$$

$$W_T(x) = \frac{3(\sin x - x \cos x)}{x^3}$$

where $|\delta_k|^2$ stands for the power spectra of the density fluctuations linearly extrapolated to the present.

It is convenient to use a simple and accurate approximation for $\sigma_{12}(q)$:

$$\frac{\sigma_{12}(q)}{(\sigma(Q))^2} \simeq e^{-b(Q)\left(\frac{q}{Q}\right)^2 - 1} \quad (5)$$

where $b(Q)$ is a coefficient depending on the the size of the halo, Q :

$$b(Q) = -\frac{1}{2} \left. \frac{d \ln \sigma(x)}{d \ln x} \right|_{x=Q}$$

If no restriction other than $\delta_l(Q) = \delta_{vir}$ were imposed on $\delta_l(q)$ the mean linear profile would be:

$$\bar{\delta}_l(q) = \int_{-\infty}^\infty P(\delta_l(q) | \delta_l(Q) = \delta_{vir}) \delta_l(q) d(\delta_l(q)) = \delta_{vir} \frac{\sigma_{12}(q)}{\sigma(Q)} \equiv \delta_0(q)$$

However, we are interested on the mean profiles satisfying also $\delta_l(q) < \delta_{vir}$ for $q > Q$. So, we must use as mean profile:

$$\bar{\delta}_l(q) = \frac{\int_{-\infty}^{\delta_{vir}} P(\delta_l(q) | \delta_l(Q) = \delta_{vir}) \delta_l(q) d(\delta_l(q))}{\int_{-\infty}^{\delta_{vir}} P(\delta_l(q) | \delta_l(Q) = \delta_{vir}) d(\delta_l(q))} \quad (6)$$

$$= \delta_0(q) - \frac{\bar{\sigma}(q) e^{-\frac{1}{2} \frac{(\delta_{vir} - \delta_0(q))^2}{(\bar{\sigma}(q))^2}}}{1 - \frac{1}{2} \text{erfc}\left(\frac{\delta_{vir} - \delta_0(q)}{\sqrt{2} \bar{\sigma}(q)}\right)}$$

$$\bar{\sigma}(q) \equiv (g(q))^{1/2}$$

For arbitrarily massive halos $\sigma(Q) \ll 1$. So, since for the relevant q values ($q > Q$) $\bar{\sigma}(q) < \sigma(Q)$, $\delta_l(q)$ is simply given by $\delta_0(q)$. However, for halos with $\sigma(Q) \gtrsim 1$, $\delta_l(q)$ is substantially steeper than $\delta_0(q)$, resulting in steeper present density profiles for smaller masses. This result has previously been advanced by Barkana (Barkana 2004) and have been confirmed by means of numerical simulations (Prada et al. 2005).

It must be noted that the profile given by expression (6) is not exactly the mean linear profile implicit in the definition of typical profile. Note that at each value of q , δ_l is constrained to lay below δ_{vir} but the probability distribution upon which this constraint is imposed does not account for the fact that the profile lies below δ_{vir} at any other value of q larger than Q . This is, however, a good approximation, because the most relevant part of the present density profile (to ≈ 10 virial radius) corresponds to a narrow region in Lagrangian coordinates ($\approx 1.5Q$). The value of δ_l for q between Q and $1.5Q$ are strongly correlated. So, if we impose the condition $\delta_l < \delta_{vir}$ at, for example, $q = 1.25Q$, the probability that the same condition holds at any q is close to one.

Once we have $\delta_l(q)$ all we need to do is to evolve it with the spherical collapse model. Using equations (3) we may write (Patiri et al.(2004) expression (20)):

$$\delta(r) = \delta(\bar{\delta}_l(q)); \quad q \equiv r [1 + \delta(r)]^{\frac{1}{3}} \quad (7)$$

where the right hand side of this equation is simply the function defined in expression (2) evaluated at $\bar{\delta}_l(q)$ (given by expression (6)). For each value of r we must solve this equation for the variable $\delta(r)$. Applying the function defined in expression (1), which is the inverse of that defined in (2), to both sides of this equation we have:

$$\delta_l(\delta(r)) = \bar{\delta}_l(q); \quad q \equiv r (1 + \delta(r))^{\frac{1}{3}} \quad (8)$$

where the left hand side is expression (1) evaluated at $\delta(r)$. This equation is usually simpler to solve than equation (7) and is the one we used in Prada et al.(2005). It must be noted, however, that, if one intends to generate the whole profile rather than to obtain $\delta(r)$ for some specific value of r , it is not necessary to solve equation (8), since one may obtain all couples of values of $\delta(r)$, r using (7) and running over all values of q . The profile obtained in this way is the typical enclosed density contrast profile, $\delta_l(r)$. To obtain the typical density contrast profile, $\delta'_l(r)$, we may use the relationship (16), given at the end of next section.

3. THE PROBABILITY DISTRIBUTION, $P(\delta, R)$. MOST PROBABLE AND MEAN PROFILES

At a given value of r , δ takes different values, $\delta(r, j)$, over the assemble of halos. The question now is which is the probability distribution of δ over this ensemble, $P(\delta, r)$. As we saw in the previous section, this can be done, in principle, by making realizations of the initial profile, $\delta_l(q, i)$, and evolving them accordingly with equations (3). Let's assume, as a first approximation, that the realizations of the initial profile may be carried out by generating for each value of q a value of δ_l accordingly with distribution (4). That is, we assume that the distribution of δ_l is only conditioned by the fact that $\delta_l(Q) = \delta_{vir}$. We shall latter consider initial profiles with an additional constraint. With these realizations we can elaborate for each value of r a histogram for $P(\delta, r)$. There is, however, a direct analytical procedure to obtain $P(\delta, r)$ from the probability distribution for δ_l (expression (4) in the present approximation).

δ is a unique function of δ_l (expression (2)). So, one may think that $P(\delta, r)$ can be obtained from (4) simply through the change of variable $\delta = \delta(\delta_l)$. However, expressions (3) show that in transforming the initial profile not only is δ_l transformed into δ , but also q is transformed into r . Now, expression (4) gives the distribution of δ_l at a fixed q value. But what we want to obtain is the distribution for δ at a fixed r value.

So, since the relationship between q and r depends on δ (or δ_l) itself, it is clear that the derivation of $P(\delta, r)$ from expression (4) (i.e. from $P(\delta_l, q)$) can not be as simple as described above.

Fortunately, there is a simple expression relating both probability distributions, which is valid as long as shell-crossing is not important:

$$P(\delta, r) = -\frac{d}{d\delta} \frac{\int_{\delta_l(\delta)}^{\delta_{vir}} P(\delta_l, q) d\delta_l}{\int_{-\infty}^{\delta_{vir}} P(\delta_l, q) d\delta_l} \quad (9)$$

$$q \equiv r (1 + \delta)^{\frac{1}{3}}$$

where $\delta_l(\delta)$ is given by expression (1) and $P(\delta_l, q)$ is the linear profile. Note that δ enters not only in the integration limit but also in the integrand through q . The derivation of this relationship is given in Patiri et al.(2004) appendix B. In that work this relationship was derived in regard with void density profiles, so it had an slightly different form. In appendix B we give the derivation corresponding to the present case.

Using expression (4) for $P(\delta_l, q)$ we find:

$$\frac{\int_{\delta_l(\delta)}^{\delta_{vir}} P(\delta_l, q) d\delta_l}{\int_{-\infty}^{\delta_{vir}} P(\delta_l, q) d\delta_l} = \frac{1}{2} \frac{\text{erfc}(F(x = \delta_l(\delta))) - \text{erfc}(F(x = \delta_{vir}))}{1 - \frac{1}{2} \text{erfc}(F(x = \delta_{vir}))} \quad (10)$$

$$F(x) \equiv \frac{x - \frac{\sigma_{12}(q)}{\sigma(Q)} \delta_{vir}}{\sqrt{2} g(q)}$$

$$q \equiv (r (1 + \delta))^{\frac{1}{3}}$$

with $\sigma_{12}(q)$, $\sigma(Q)$, $g(q)$ as defined in (4).

For the purposes of this section we may neglect the term $\text{erfc}(F(x = \delta_{vir}))$. The full expression shall be used in section 5 along with a more refined one. We then have:

$$P(\delta, r) = \frac{1}{\sqrt{\pi}} e^{-F^2(x = \delta_l(\delta))} \frac{d}{d\delta} F(x = \delta_l(\delta)) \quad (11)$$

By construction, δ at r must be smaller than Δ_{vir} and larger than certain value, $\delta_{min}(r)$:

$$\delta_{min}(r) = 341 (R_{vir}/r)^3 - 1 \quad (12)$$

This minimum value corresponds to a situation where there is no matter in between R_{vir} and r . So, for δ values outside the interval $(\delta_{min}(r), \Delta_{vir})$, $P(\delta, r)$ is zero.

We may obtain an analytical expression for $P(\delta, r)$ using approximation (5) for $\frac{\sigma_{12}(q)}{\sigma_1^2}$ and the following approximation for $\sigma(q)$ (which enters $g(q)$, defined below expression (4)):

$$\sigma(q) \simeq (1.65 \cdot 10^{-2} + 0.105(q h \text{ Mpc}^{-1}))^{-\frac{1}{2}} \quad \text{for } q < 3 h^{-1} \text{ Mpc}$$

As mentioned before, expression (9) is valid as long as shell-crossing is not important. In Prada et al.(2005) we have found by mean of comparison with numerical simulations that, beyond three virial radius, the relevance of shell-crossing diminishes quickly. This relevance can be estimated a priori (i.e. without comparison with simulations) obtaining $P(\delta, r)$ directly through realizations of the initial profile accordingly with expression (4) and evolving them accordingly with equations (3). If shell-crossing were irrelevant, the $P(\delta, r)$ obtained in this way should be equal to that given by expression (11). The presence of certain amount of shell-crossing

will cause the $P(\delta, r)$ obtained with realization to have a somewhat smaller maxima and a more extended tail than that given by (11) (note that it is this expression that corresponds to realizations elaborated with expression (4). In this case none of the procedures gives the correct $P(\delta, r)$ because both assume that δ is related to δ_l by means of expression (1), which is inconsistent when shell-crossing is important. However, the difference between the results obtained with both procedures is of the same order of the difference between any of them and the profile obtained with a proper treatment of shell-crossing. Note that even this last $P(\delta, r)$ is not the real one, since, as we said before, we are generating the initial profile using only a two point distribution (expression (4)).

In figure 1 we compare the $P(\delta, r)$ obtained by the two procedures mentioned above for several values of r expressed in unit of the virial radius (that we denote by s). We also show the corresponding histograms obtained from the numerical simulations described in Prada et al.(2005), which were done using the Adaptive Refinement Tree (ART) code (Kravtsov et al. 1997) for the standard Λ CDM cosmological model with $\Omega_0 = 0.3$, $\Omega_\Lambda = 0.7$, $h = 0.7$, and cover a wide range of scales with different mass and force resolutions (see Prada et al. 2005 for a detailed description). In particular, the histograms in figure 1 were obtained for a total of 654 halos in a mass range of $3 \pm 1 \cdot 10^{12} h^{-1} M_\odot$ selected without any kind of isolation criteria.

We can see that, for $s = 2.5$, where shell-crossing is already important, there is substantial difference between the results of both procedures. A considerable amount of probability is transferred from the most probable value to much larger values ($\delta \approx 100$) causing the distribution obtained through the realizations to be bimodal. For $s = 3.5$ there is still a small amount of shell-crossing causing the maxima obtained with both procedures to differ by roughly a 20%. For larger values of s this difference steadily diminishes.

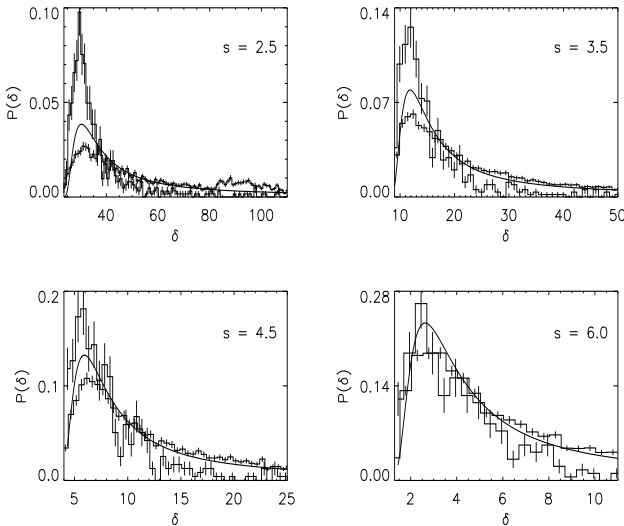


FIG. 1.— $P(\delta, r)$ as given by expression (11) compared with the corresponding histogram obtained through realizations (histogram with small error bars) and that found in the simulations (histogram with large error bars) for four values of s ($\equiv r/R_{vir}$) and a mass of $3 \times 10^{12} h^{-1} M_\odot$ ($\Delta_{vir} = 340$ and $\delta_{vir} = 1.9$).

Furthermore, as s increases the difference between the distribution given by expression (11) and the histogram obtained

with the numerical simulations reduces. In fact, even for $s = 3.5$ the relative values of $P(\delta, r)$ at different values of δ to the left of the maxima are very well given by (11). The difference in the absolute values with respect to those in the histogram is due to the normalization. For δ values to the right of the maxima, expression (11) gives a considerably more extended tail than in the actual distribution. Therefore the normalization constant is larger in the latter case.

Note that, although the maxima of expression (11) and that of the histogram corresponding to the numerical simulations approach as s increases, due to the increasing irrelevance of the tail, this tail is still substantially more extended even for $s = 6$. Now, since the relevance of shell-crossing is small for s larger than 3, the most likely explanation for the excess in the tail given by expression (11) lies on the fact that we are using expression (4) for $P(\delta_l, q)$. In the last section we shall consider a better $P(\delta, r)$ and discuss the resulting improvement of the behaviour of its tail.

Using $P(\delta, r)$ (as given by (11)) we may immediately obtain the most probable and the mean profiles. For the first one we have:

$$\delta_p(r) \equiv \delta_{max}; \quad \left. \frac{d}{d\delta} P(\delta, r) \right|_{\delta=\delta_{max}} = 0 \quad (13)$$

And for the mean profile, in principle:

$$\bar{\delta}(r) \equiv \int_{\delta_{min}}^{\Delta_{vir}} P(\delta, r) \delta d\delta \quad (14)$$

However, due to the fact that the mean is rather sensitive to the form of the tail, we must artificially cut off the tail. From the simulations we know that the real tail practically ends at $\delta \sim \delta_0(r)$ with δ_0 given by:

$$P(\delta_0, r) = \frac{P(\delta_{max}, r)}{25}$$

So, instead of (14) we use (Prada et al.2005):

$$\bar{\delta}(r) \equiv \frac{\int_{\delta_{min}}^{\delta_0(r)} P(\delta, r) \delta d\delta}{\int_{\delta_{min}}^{\delta_0(r)} P(\delta, r) d\delta} \quad (15)$$

In table 1 we give the values of δ_0 and δ_{max} for several values of s ($\equiv r/R_{vir}$).

So far we have considered the probability distribution and profiles of the spherically-averaged enclosed density contrast, δ . We shall now consider the local density contrast δ' , that is the density contrast within a narrow shell of radius r . In this case we can not obtain $P(\delta', r)$ by mean of a simple relationship like expression (9). However, the mean δ' profile can be obtained from the mean δ profile. To this end, note that for each actual density profile, that is, for each spherically evolved realization of the linear profile, $\delta(r, j)$, the following relationship holds:

$$\delta'(r, j) = \frac{1}{3r^2} \frac{d}{dr} (r^3 \delta(r, j)) \quad (16)$$

which follows immediately from the definitions of δ , δ' . The mean δ profile does not correspond to any actual density profile. However, being the mean a linear operation, the same relationship holds for the mean profiles:

$$\bar{\delta}'(r) \equiv \langle \delta'(r, j) \rangle_j = \langle \frac{1}{3r^2} \frac{d}{dr} (r^3 \delta(r, j)) \rangle_j \quad (17)$$

$$= \frac{1}{3r^2} \frac{d}{dr} (r^3 < \delta(r, j) >_j) = \frac{1}{3r^2} \frac{d}{dr} (r^3 \bar{\delta}(r))$$

TABLE 1
ARTIFICIAL CUT-OFF FOR $P(\delta, r)$

s	δ_{max}	δ_0
1.5	115.2	495.4
2.5	28.6	135.3
3.5	11.3	67.9
4.5	5.8	42.2
5.5	3.3	29.3
6.5	2.0	19.6
7.5	1.3	12.8
8.5	0.82	8.1

The most probable profile is constructed with the ensemble of profiles $\delta(r, j)$ by means of a non-linear operation: that of choosing, for any value of r , the member of the ensemble with the largest probability density for $\delta(r)$. So, relationship (16) is not valid between δ'_p and δ_p , because the value of δ_p at different values of r may correspond to different members of the ensemble. However, in Prada et al.(2005) we have used expression (16) to obtain $\delta'_p(r)$ from $\delta_p(r)$ and found results in good agreement with the simulations, but this is a posteriori agreement: unlike the prediction for $\bar{\delta}'(r)$, the value of $\delta'_p(r)$ obtained using expression (16) is not a proper prediction.

4. RADIAL VELOCITY PROFILE OF DARK MATTER HALOS

In the spherical collapse model, the radial velocity at distance r with respect to the center of the spherical cloud is a unique function of the spherically-averaged enclosed density contrast, $\delta(r)$. An exact analytical expression may be given for this relationship using $\delta_l(\delta)$ (expression (1)). Mass conservation within a shell with initial Lagrangian radius q , implies that, at any time, the following relationship must hold:

$$\frac{r(t)}{a(t)} = q(1 + \delta)^{-\frac{1}{3}} \quad (18)$$

where $a(t)$ is the scale factor of the universe (normalized to 1 at present) so that the left hand side is the comoving radii of that shell at time t . Deriving this equation with respect to time we find:

$$\frac{\dot{r}(t)}{a(t)} - \frac{\dot{a}(t)}{a^2(t)} r(t) = \frac{\dot{r}(t) - H(t) r(t)}{a(t)} = -\frac{1}{3} q(1 + \delta)^{-\frac{4}{3}} \dot{\delta} \quad (19)$$

where $H(t)$ is the Hubble constant. Using now $\delta(\delta_l)$ we may express $\dot{\delta}$ in the form:

$$\dot{\delta} = \frac{d\delta(\delta_l)}{d\delta_l} \dot{\delta}_l; \quad \dot{\delta}_l = \frac{\dot{D}(t)}{D(t)} \delta_l = \frac{a(t)}{D(a(t))} \frac{dD(a(t))}{da(t)} H \delta_l \quad (20)$$

where $D(t)$ is the growing mode of linear density fluctuations. Now, since $\delta(\delta_l)$ is the inverse function of $\delta_l(\delta)$ we have:

$$\frac{d\delta(\delta_l)}{d\delta_l} = \left(\frac{d\delta_l(\delta)}{d\delta} \right)^{-1}$$

Using this in (20), inserting (20) in (19) and using again (18) we find:

$$V_r \equiv \dot{r} = H(t) r - \frac{1}{3} \frac{a(t)H}{D(a(t))} \frac{dD(a(t))}{da(t)} \frac{r}{(1 + \delta)} \frac{\delta_l(\delta)}{\frac{d\delta_l(\delta)}{d\delta}} \equiv r f(\delta) \quad (21)$$

For the concordant cosmology we have at present $H = 72 \text{ km/s/Mpc}$, $a = 1$, $\frac{dD(a)}{da}/D(a) = 0.51$. Writing (21) in the form $V_r = r f(\delta)$ we may use expression (11) to obtain the probability distribution, $P(V_r, r)$, for V_r at radii r :

$$P(V_r, r) = P\left(\delta = f^{-1}\left(\frac{V_r}{r}\right), r\right) \left(\frac{df(\delta)}{d\delta}\right)^{-1} \frac{1}{r} \quad (22)$$

where f^{-1} is the inverse function of f and where $P(\delta, r)$ is given by expression (11).

This distribution should not be confused with the distribution for the radial velocity of dark matter particles at a given value r . V_r is the mean radial velocity of all particles in a given narrow shell with radius r . So, for a given halo and a given value of r , V_r takes a unique value. Expression (22) gives the distribution of this value over the ensemble of halos.

The mean V_r profile is given by:

$$\bar{V}_r = \frac{\int_{\delta_{min}}^{\delta_0(r)} P(\delta, r) r f(\delta) d\delta}{\int_{\delta_{min}}^{\delta_0(r)} P(\delta, r) d\delta} \quad (23)$$

with $P(\delta, r)$ given by (11), δ_0 as given in Table 1, $f(\delta)$ given by (21) and δ_{min} given by (12).

In figure 2 we show the predictions given by (23) for the mean radial velocity profile, and compare it with the profile:

$$V_r \equiv r f(\bar{\delta}(r)) \quad (24)$$

That is, for each value of r , this expression gives V_r corresponding to the mean δ at that r through Eq.(21). We find that Eq.(24) is a good approximation to Eq.(23).

Note that, although we have used the probability distribution given by Eq.(11), these expressions are valid for any $P(\delta, r)$.

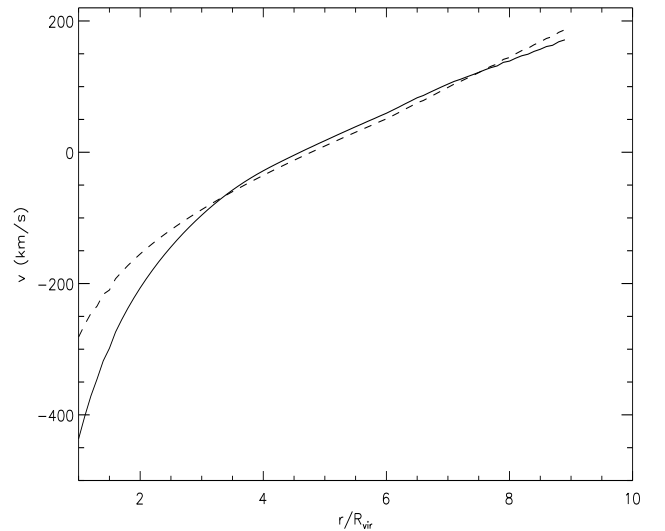


FIG. 2.— Radial velocity profile as given by expression (23) (filled line) and as given by expression (24) (dashed line). Both correspond to a mass of $3 \times 10^{12} h^{-1} M_\odot$

5. IMPROVING $P(\delta, R)$

We have seen that for $s (= r/R_{vir})$ larger than 3 the realization of initial profiles and their subsequent evolution lead to values of $P(\delta, r)$ very close to those obtained using expression (11). This means that shell crossing is not important at these radii. So, the difference between the actual value of $P(\delta, r)$ (the histogram obtained from the simulations) and that given by expression (11) lies on the fact that this expression is only an approximation, or in the possible relevance of triaxiality, non-radial motions and pressure (velocity dispersions). To determine the amount of the discrepancy due to inaccuracies in the statistical description of the initial conditions as opposed to the discrepancy due to neglected dynamical factors, we must consider better approximation than that provided by expression (11). We shall use now two improved approximations. The first one is that obtained by using expression (10) in expression (9), which we represent by $P_1(\delta, r)$. Note that, to derive this approximation we have used the fact that at a given q larger than Q , δ_l must be smaller than δ_{vir} , but we have used expression (4) for $P(\delta_l, q)$. This distribution does not account for the fact that for all values of q larger than Q , $\delta_l < \delta_{vir}$. Consequently, $P(\delta_l, q)$ falls off with δ_l more slowly than it should and the same applies to $P(\delta, r)$. In the second approximation, which we represent by $P_2(\delta, r)$, we consider a $P(\delta_l, q)$ which takes into account this additional constraint. By comparing the predictions obtained with $P_2(\delta, r)$, $P_1(\delta, r)$ with those obtained with $P(\delta, r)$ (expression (11)) we may check whether $P_1(\delta, r)$ is accurate enough, so that the remaining discrepancy of the prediction with the results shown in the simulations may be ascribed to unaccounted dynamical factors.

We have already pointed out that the most relevant part of the present density profile (up to ~ 8 virial radii) comes from a narrow band in Lagrangian coordinates (from Q to $\sim 1.5Q$) so that the values of δ_l within this band are strongly correlated. This is the reason why using expression (4) for $P(\delta_l, q)$ is a good approximation, because if δ_l at q (within the mentioned band) lies below δ_{vir} the same will probably be valid also at all q' larger than Q . We go now a step further and explicitly demand that δ_l lies below δ_{vir} at all Lagrangian radii in between Q and q . Imposing the same condition at q' larger than q is unnecessary since it will lead to a negligible change for $P(\delta_l, q)$, because if δ_l lies below δ_{vir} at q the same will almost certainly occur at larger distances.

Given the strong correlation between the values of δ_l in between Q and q (for the relevant q 's), the condition that for all values of q larger than Q $\delta_l < \delta_{vir}$, is almost equivalent to demanding that δ_l lies below δ_{vir} at the middle point $q' = \frac{1}{2}(q + Q)$. We might have chosen any other point in between and searched for the point imposing the strongest constraint, since the real constraint must be stronger (i.e. the tail of the distribution falls off more steeply) than that imposed by the point leading to the strongest constraint. We have chosen the middle point because it seems a priori a good choice.

Here we discuss the main lines of the derivation and the result for $P(\delta_l, q)$ within this new condition, which we represent by $P_2(\delta_l, q)$. We give in appendix A the details and the full descriptions of the expressions involved.

To obtain $P_2(\delta_l, q)$ we must first obtain the joint probability distribution for the value of δ_l at Q , the middle point, and at q . We represent by x_1, x_2, x_3 respectively the value of δ_l at these three points.

The joint distribution for these three variables is a Gaussian trivariate distribution $P(x_1, x_2, x_3)$, which can be obtained for

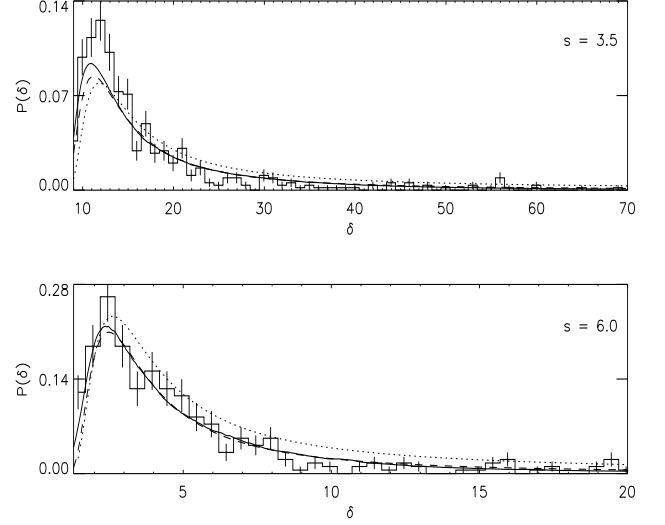


FIG. 3.— Probability distribution for δ at 3.5 and 6 virial radius for $3 \times 10^{12} h^{-1} M_\odot$. The filled curve corresponds to the approximation given by expression (26), the dashed curve to that given by full expression (9), and the dotted curve to expression (11). The histogram corresponds to the same simulations as in fig. 1.

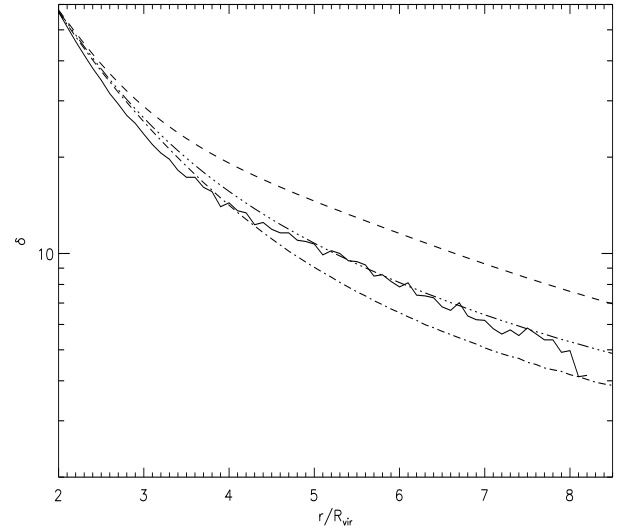


FIG. 4.— Mean δ profile for $3 \times 10^{12} h^{-1} M_\odot$ using the probability distribution given by expression (11) (dashed line), by full expression (9) (3-dots-dashed line) and by expression (26) (dot-dashed line). Mean δ obtained from simulations is given for comparison (filled line). In all the cases, a maximum value of $\delta = 70$ was used.

a given power spectra. With this distribution we may immediately obtain the distribution of x_3 conditioned to $x_1 = \delta_{vir}$, $x_2 < \delta_{vir}$, namely: $\bar{P}_2(\delta_l, q)$. So, we have:

$$\bar{P}_2(\delta_l, q) = \frac{\int_{-\infty}^{\delta_{vir}} P(x_2|x_1) P(x_3|x_1, x_2) dx_2}{\int_{-\infty}^{\delta_{vir}} P(x_2|x_1) dx_2} \quad (25)$$

where $P(\delta_{vir}, x_2)$ is the joint probability distribution for x_1, x_2 with $x_1 = \delta_{vir}$. $\bar{P}_2(\delta_l, q)$ is the probability distribution of δ_l at q conditioned to $\delta_l(Q) = \delta_{vir}$ and $\delta_l(q') < \delta_{vir}$. We have not imposed yet the almost redundant condition (since $\bar{P}_2(\delta_l, q)$ is very small for $\delta_l > \delta_{vir}$) that δ_l at q must be smaller than δ_{vir} . The probability distribution for δ_l with this condition,

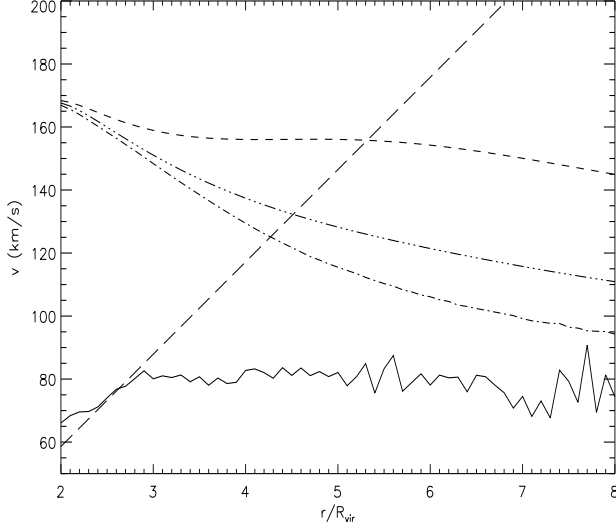


FIG. 5.— Peculiar infall velocity profile for $3 \times 10^{12} h^{-1} M_{\odot}$ using the probability distribution given by expression (11) (dashed line), by full expression (9) (3dots-dashed line) and by expression (26) (dot-dashed line). Peculiar infall velocity profile obtained from simulations is given for comparison (filled line). In all the cases, a maximum value of $\delta = 70$ was used. The straight line corresponds to the Hubble Flow.

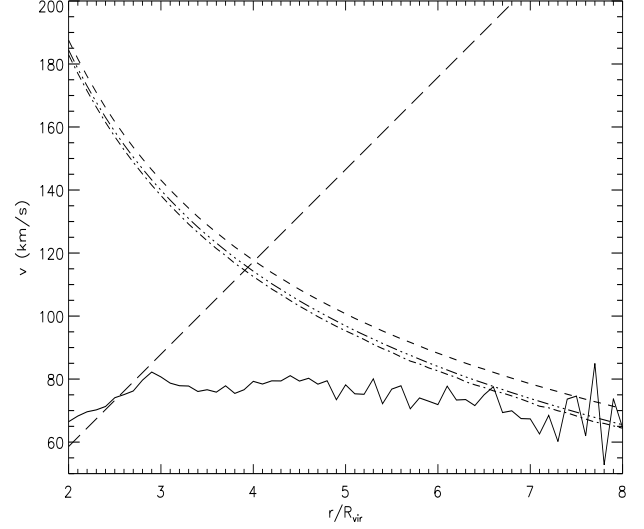


FIG. 7.— Peculiar infall velocity profile for $3 \times 10^{12} h^{-1} M_{\odot}$ using the probability distribution given by expression (11) (dashed line), by full expression (9) (3dots-dashed line) and by expression (26) (dot-dashed line). Peculiar infall velocity profile obtained from simulations is given for comparison (filled line). For all radius, the average was calculated excluding the 20% of the halos with the largest δ values. The straight line corresponds to the Hubble Flow.

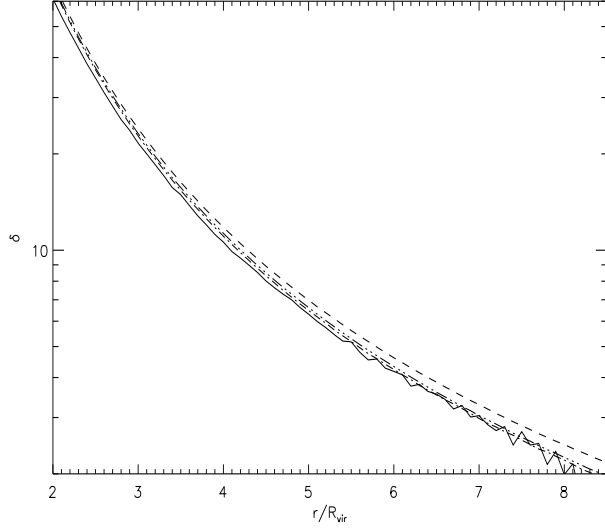


FIG. 6.— Mean δ profile for $3 \times 10^{12} h^{-1} M_{\odot}$ using the probability distribution given by expression (11) (dashed line), by full expression (9) (3dots-dashed line) and by expression (26) (dot-dashed line). Mean δ obtained from simulations is given for comparison (filled line). For all radius, the average was calculated excluding the 20% of the halos with the largest δ values.

$P_2(\delta_l, q)$, is simply obtained through normalization (see (A5))

The distribution for δ at fixed r within this formalism, which we represent by $P_2(\delta, r)$, may be obtained from $P_2(\delta_l, r)$ by means of expression (9), which is valid when shell-crossing is not important ($s \gtrsim 3$):

$$P_2(\delta, r) = -\frac{d}{d\delta} \int_{\delta_l(\delta)}^{\delta_{vir}} P_2(\delta_l, q) d\delta_l \quad (26)$$

$$q \equiv r(1+\delta)^{\frac{1}{3}}$$

In figure 3 we show the probability distributions for a mass of $3 \times 10^{12} h^{-1} M_{\odot}$ at 3.5 and 6.0 virial radius. As expected,

$P_2(\delta, r)$ falls off much faster than $P(\delta, r)$ being in excellent agreement with the simulations. The tail of $P_1(\delta, r)$ falls off sufficiently fast to give sensible results for the density and velocity profiles averaged over all possible halos (δ between δ_{min} and Δ_{vir}). However, we know that for $\delta \gtrsim 70$ the standard spherical collapse model is not a good approximation, so we can not learn much by comparing simulations with predictions for averages over all halos. It is more instructive to compare the predictions for the averages corresponding to δ values between δ_{min} (expression (12)) and 70 with those found in the simulations for the same range of δ values.

In figure 4 we show the predictions given by $P(\delta, r)$, $P_1(\delta, r)$, $P_2(\delta, r)$ for the δ profile averaged between δ_{min} and 70 and the averaged found in the simulations. In figure 5 the corresponding results for the peculiar infall velocity (the Hubble Flow minus the radial velocity) are presented. One of the things we learn from these figures is that $P_2(\delta, r)$ must differ very little from the exact distribution, since it may be shown on general grounds that the difference between the predictions given by these two distributions must be much smaller than the difference between the predictions given by $P_2(\delta, r)$ and $P_1(\delta, r)$. Another thing that we learn is that the spherical collapse model can not be a good approximation for all halos included in the averaging process. The reason being that only the presence of some considerably triaxial haloes (i.e. haloes such that the density contours of their outskirts are very triaxial) within the averaging assemble can explain the fact that the results found in the simulations are somewhat larger than those obtained using $P_2(\delta, r)$. If the dynamical factor that we have neglected were irrelevant the latter results must be slightly above the former. Non-radial motion and velocity dispersions preserve the order, only increasing the difference. The reason being that when these factors are taken into account, while preserving spherical symmetry, $\delta_l(\delta)$ is steeper (δ smaller for given δ_l) than in the standard model (expression (1)), resulting, through expression (26) and (A8) in steeper $\bar{\delta}(r)$. So, only the relevance of triaxiality can explain

the results shown in figure 4. The effect is not large in this figure, since only a small fraction of the halos are affected, but it is quite meaningful. It is this very effect that is causing that the peculiar infall velocity profile predicted by means of $P_2(\delta, r)$ does not agree with that found in the simulations even at $r/R_{vir} \gtrsim 7$.

Knowing that for some halos the spherical collapse model can not be a good approximation, the relevant question now is to determine precisely how good is it for most halos. To this end, at each radial bin we search for the value, $\delta_1(r)$, such that the upper cumulative probability, as given by $P_2(\delta, r)$, is 0.2, and eliminate, both in the simulations and in the predictions, halos with larger δ values at that bin. By doing so, we eliminate many halos which simply have flatter profiles than average, but are otherwise sufficiently spherical for the model to apply. But, we are sure of having eliminated all halos with highly triaxial outskirts, most of them corresponding to situations where a couple of halos lie within a few virial radius from each other, so that each of them will show up in the outskirts of the other halo; a situation that, by no mean, can be described by the spherical model. The resulting profiles, as given by the different approximations to $P(\delta, r)$ and the simulations are given in figure 6. The difference between the various approximations is now smaller, since the main difference occurs at the far tail (of $P(\delta, r)$), which has now been eliminated, but this difference increases for smaller masses. The profile obtained from the simulations lies now slightly below the best prediction, as it should be if the spherical model is a good approximation. In figure 7 we show the corresponding results for the peculiar infall velocity. It is apparent that the prediction agrees well with the simulations at large radii but as we go below ~ 5 virial radius there is an increasing discrepancy. This must be due to the unaccounted dynamical factors.

Figure 8 give us another clue as to the relative effect of these factors. Triaxiality causes the dispersion of δ at any given radii to increase, since, for a given value of δ_l triaxial evolution gives a distribution of δ values with a finite dispersion, while the spherical model gives a single value. So, the fact that the dispersion found in the simulations lies somewhat below the predictions, imply that triaxiality can not be dominant amongst unaccounted factors.

In summary, the distribution $P_2(\delta, r)$ is very close to the exact. To most purposes the simpler distribution $P_1(\delta, r)$ may be used, their difference being small, although it increases for smaller values. The density profiles obtained with $P_2(\delta, r)$ are in excellent agreement with those found in simulations beyond ~ 3 virial radius. The density dispersion and the radial velocity show some discrepancy below ~ 5 virial radius, which clearly indicate the relevance of unaccounted dynamical factors, specially velocity dispersions.

6. FINAL REMARKS

The spherical collapse model describes very well the properties of dark matter halos beyond three virial radius. This could seem surprising given the fact that the density contours around halos may be considerably aspherical and the presence of tidal fields.

Nevertheless, the assumption that the spherically averaged density profiles at several virial radius evolves according with

the spherical collapse model is not just a simplification introduced to make the problem tractable. The mean evolution is given by the spherical collapse model with some dispersion (for a given δ_l) due to triaxiality. This have been

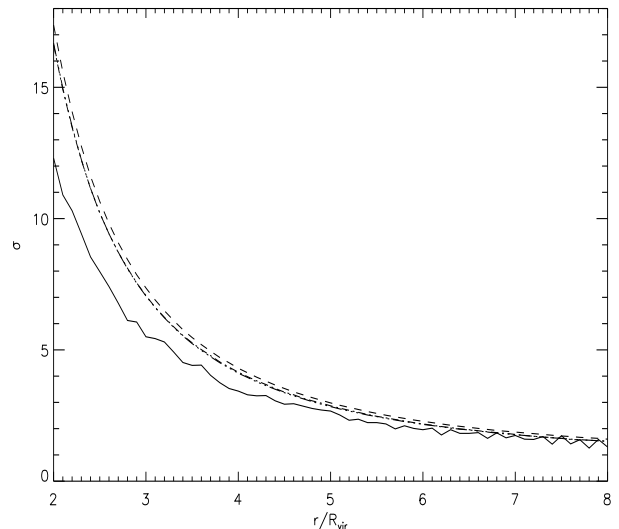


FIG. 8.— σ corresponding to the mean δ profiles (excluding at each radius the upper 20% δ values) obtained using different probability distributions, as shown in fig.6 (same type of lines used here); σ of the mean δ obtained from simulations is also given for comparison (filled line).

shown by mean of simulations (Lilje et al. 1986) and analytical works (Bernardeau 1994). At sufficiently large radii where δ is sufficiently small ($\delta \lesssim 10$) the fractional dispersion becomes small. At small radii, not only the dispersion becomes larger, causing the mean value of δ for a given δ_l to be somewhat different from $\delta(\delta_l)$ (expression (1)), but also the effect of non-radial motions and velocity dispersions starts to dominate. So studying the dark matter profile where the uncertainty of the evolution is small, we may check that the initial conditions we use are correct to a high degree of accuracy. With these conditions, as described by the most accurate probability distribution, $P_2(\delta_l, q)$, we should be able to obtain very accurate predictions for all possible definitions (typical, mean...) of density and velocity profile. That is, there is no room for remodeling; all properties must be explained with one and the same $P_2(\delta_l, q)$. Any residual discrepancy should be explained by triaxiality, non-radial motions and velocity dispersions, as we shall show in a future work, although, from the results shown in this work, the last two effects dominate at least up to roughly 5 virial radius. Going a step further, if we adequately take into account the neglected dynamical factors, the same initial conditions should explain the profile at any radii. In this way, we could be able to explain the dark matter profiles at least down to a virial radii understanding the role played by the initial conditions and by the different processes relevant to the evolution.

ACKNOWLEDGMENTS

M.A. thanks support from the Spanish MEC under grant PNAYA 2002-01241. We also thank support from MEC under grant PNAYA 2005-07789.

APPENDIX

DERIVATION OF $P_2(\delta_L, Q)$

The field of initial density fluctuations linearly extrapolated to the present $\delta_l(\vec{q})$ is a random Gaussian field. Any set of quantities obtained through a linear operation on a Gaussian field follows a Gaussian multivariate distribution. The quantities we are interested in are the average of the linear field within three concentric spheres centered at a randomly chosen point with Lagrangian coordinate \vec{q} . The Lagrangian radius of these spheres are Q , $\frac{1}{2}(Q+q)$, q (note that q is not the norm of \vec{q}) and we represent the average of the linear field within them by $x_1(\vec{q})$, $x_2(\vec{q})$, $x_3(\vec{q})$ respectively. These are three random Gaussian fields, but their values at a randomly chosen \vec{q} we represent simply by x_1 , x_2 , x_3 . Their joint distribution is a Gaussian tri-variate:

$$P(x_1, x_2, x_3) = \frac{e^{-\frac{1}{2}\chi}}{(2\pi)^{\frac{3}{2}} |\det \mathbf{C}|}$$

$$\chi = \sum_{i,j=1}^3 (\mathbf{C}^{-1})_{jj} x_i x_j; \quad (\mathbf{C})_{ij} \equiv \langle \mathbf{x}_i \mathbf{x}_j \rangle$$

where \mathbf{C}^{-1} is the inverse matrix of \mathbf{C} , whose diagonal elements are the variances of the x 's and the other elements are their correlations.

Using the definitions of the probability distribution for x_2 conditioned to a given value of x_1 , $P(x_2|x_1)$, and of the distribution for x_3 conditioned to given values of x_1 , x_2 , $P(x_3|x_1, x_2)$, we may write:

$$P(x_1, x_2, x_3) = P(x_1) P(x_2|x_1) P(x_3|x_1, x_2) \quad (\text{A1})$$

Now, by grouping terms in χ in an appropriate manner we infer that:

$$P(x_1) = \frac{e^{-\frac{x_1^2}{2\sigma_1^2}}}{\sqrt{2\pi} \sigma_1}$$

$$P(x_2|x_1) = \frac{e^{-\frac{(x_2 - P x_1)^2}{2g}}}{\sqrt{2\pi} g^{\frac{1}{2}}}$$

$$g \equiv \sigma_2^2 (1 - \bar{c}_{12}^2); \quad P \equiv \bar{c}_{12} \frac{\sigma_2}{\sigma_1}$$

$$P(x_3|x_1, x_2) = \frac{e^{-\frac{(x_3 - A x_1 - B x_2)^2}{2\sigma'^2}}}{\sqrt{2\pi} \sigma'}$$

$$\sigma'^2 \equiv \sigma_3^2 \frac{(1 + 2\bar{c}_{12} \bar{c}_{13} \bar{c}_{23} - (\bar{c}_{12}^2 + \bar{c}_{13}^2 + \bar{c}_{23}^2))}{(1 - \bar{c}_{12}^2)}; \quad A \equiv -\frac{\bar{c}_{12} \bar{c}_{23} - \bar{c}_{13}}{1 - \bar{c}_{12}^2} \frac{\sigma_3}{\sigma_1}; \quad B \equiv -\frac{\bar{c}_{12} \bar{c}_{13} - \bar{c}_{23}}{1 - \bar{c}_{12}^2} \frac{\sigma_3}{\sigma_2}$$

$$\bar{c}_{ij} \equiv \frac{\langle x_i x_j \rangle}{\sigma_i \sigma_j}; \quad \sigma_i \equiv \sigma(q_i)$$

$$q_1 = Q; \quad q_2 = \frac{1}{2}(Q+q); \quad q_3 = q$$

$\sigma(q)$ is the linear RMS density fluctuation as a function of Lagrangian radii (see expression (4)). $\langle x_i x_j \rangle$ is what we called σ_{ij} in expression (4), with q_i , q_j in the place of q , Q :

$$\sigma_{ij} = \sigma_{ij}(q_i) = \frac{1}{2\pi^2} \int_0^\infty |\delta_k|^2 W_T(q_i k) W_T(q_j k) k^2 dk \quad (\text{A3})$$

We may now obtain the distribution for x_3 conditioned to $x_1 = \delta_{vir}$, $x_2 < \delta_{vir}$:

$$P(x_3|x_1 = \delta_{vir}, x_2 < \delta_{vir}) = \frac{\int_{-\infty}^{\delta_{vir}} P(x_2|x_1) P(x_3|x_1, x_2) dx_2}{\int_{-\infty}^{\delta_{vir}} P(x_2|x_1) dx_2} \quad (\text{A4})$$

Note that $P(x_1)$ cancels.

Using (A2) and rearranging terms in the exponent we may write:

$$P(x_2|x_1) P(x_3|x_1, x_2) = \frac{1}{2\pi g^{\frac{1}{2}} \sigma'} \exp \left[-\frac{(x_3 - Ax_1)^2}{2\sigma'^2} - \frac{P^2 x_1^2}{2g} + \frac{\left(\frac{Px_1}{2g} + \frac{Bx_3}{2\sigma'^2} - \frac{ABx_1}{2\sigma'^2}\right)^2}{\left(\frac{B^2}{2\sigma'^2} + \frac{1}{2g}\right)} \right] \times \\ \times \exp \left[-\left(\frac{B^2}{2\sigma'^2} + \frac{1}{2g}\right) \left(x_2 - \frac{\left(\frac{Px_1}{2g} + \frac{Bx_3}{2\sigma'^2} - \frac{ABx_1}{2\sigma'^2}\right)}{\left(\frac{B^2}{2\sigma'^2} + \frac{1}{2g}\right)}\right)^2 \right]$$

x_2 appears only in the second factor and both integrals in (A4) can directly be expressed in terms of the error complementary function:

$$P(x_3|x_1 = \delta_{vir}, x_2 < \delta_{vir}) = \frac{1}{2\sqrt{\pi} g^{\frac{1}{2}} L^{\frac{1}{2}} \sigma'} \exp \left[-\frac{(x_3 - A\delta_{vir})^2}{2\sigma'^2} - \frac{P^2 \delta_{vir}^2}{2g} + \frac{U^2}{L} \right] \times \\ \times \left[1 - \frac{1}{2} \operatorname{erfc} \left(\left(\delta_{vir} - \frac{U}{L} \right) L^{\frac{1}{2}} \right) \right] \times \left[1 - \frac{1}{2} \operatorname{erfc} \left(\frac{\delta_{vir} (1-P)}{\sqrt{2} g^{\frac{1}{2}}} \right) \right]^{-1} \\ U \equiv \frac{\delta_{vir} P}{2g} + \frac{B x_3}{2\sigma'^2} - \frac{AB\delta_{vir}}{2\sigma'^2} \\ L \equiv \frac{B^2}{2\sigma'^2} + \frac{1}{2g}$$

$\overline{P}_2(\delta_l, q)$, as defined in the text, is given by:

$$\overline{P}_2(\delta_l, q) = P(x_3 = \delta_l | x_1 = \delta_{vir}, x_2 < \delta_{vir})$$

So, $P_2(\delta_l, q)$, which is simply $\overline{P}_2(\delta_l, q)$ with the restriction: $\delta_l < \delta_{vir}$ and the corresponding normalization, is given by:

$$P_2(\delta_l, q) = \begin{cases} \frac{P(x_3 = \delta_l | x_1 = \delta_{vir}, x_2 < \delta_{vir})}{\int_{-\infty}^{\delta_{vir}} P(x_3 = \delta_l | x_1 = \delta_{vir}, x_2 < \delta_{vir})} & \text{if } \delta_l < \delta_{vir} \\ 0 & \text{if } \delta_l \geq \delta_{vir} \end{cases} \quad (\text{A5})$$

Note that the right hand side in the case $\delta_l > \delta_{vir}$ depends on q through σ_i, \bar{c}_{ij} . These quantities may be computed directly with arbitrary precision evaluating the integral entering their definition (expression (A2)). However, to be able to obtain efficiently $P_2(\delta, r)$, we need accurate fits to these quantities as a function of q . It is very difficult, however, to obtain consistent approximation for these quantities: very small errors in \bar{c}_{ij} may lead to inconsistent result, for example, negative values for σ'^2 . So, it is more expedient to fit directly the quantities (A, B, P, σ'^2) where the σ_i, \bar{c}_{ij} enter. We find the following fits:

$$A = \left(-e^{-1.386 b \left(\left(\frac{q}{\bar{\varrho}} \right)^2 - 1 \right)} \right) \frac{\sigma_3}{\sigma_1}; \quad B = \left(1 + e^{-1.504 b \left(\left(\frac{q}{\bar{\varrho}} \right)^2 - 1 \right)} \right) \frac{\sigma_3}{\sigma_2}; \quad P = e^{-0.475 b \left(\left(\frac{q}{\bar{\varrho}} \right)^2 - 1 \right)} \quad (\text{A6}) \\ \sigma'^2 = \sigma_3^2 \frac{6.63 \cdot 10^{-2} b^4 \left(\left(\frac{q}{\bar{\varrho}} \right)^2 - 1 \right)^4}{1 - \left(\frac{\sigma_1}{\sigma_2} P \right)^2}$$

where b is as defined in expression (4) ($b = 0.2544$ for $M = 3 \times 10^{12} h^{-1} M_\odot$). This fit is valid in the range 3×10^{11} to $3 \times 10^{13} h^{-1} M_\odot$. Outside this range it may be necessary using the full expressions (A2) or a different fit to them.

Using expression (A5) in expression (26) we find:

$$P_2(\delta, r) = -\frac{d}{d\delta} G(\delta, q = r(1+\delta)^{\frac{1}{3}}) \quad (\text{A7})$$

with:

$$G(\delta, q) = \int_{\delta_l(\delta)}^{\infty} P_2(\delta_l, q = r(1+\delta)^{\frac{1}{3}}) d\delta_l$$

where the dependence on q enters through the coefficients.

Inserting expression (A7) into expressions (14) and (23) in the place of $P(\delta, r)$, we may obtain the values of $\bar{\delta}(r)$, $\bar{V}(r)$ (the average corresponding to δ values between δ_{min} and δ_{max}) as given by our best approximation to the probability distribution for δ at a given r . After integrating by parts we find:

$$\bar{\delta}(r) = \int_{\delta_{min}}^{\delta_{max}} G(\delta, r) d\delta - \delta_{min} - \delta_{max} G(\delta_{max}, r) \\ \bar{V}_r(r) = r \left(\int_{\delta_{min}}^{\delta_{max}} f'(\delta) G(\delta, r) d\delta + f(\delta_{min}) - f(\delta_{max}) G(\delta_{max}, r) \right) \quad (\text{A8})$$

where $f'(\delta)$ stands for the derivative of $f(\delta)$ (defined in expression (21)) with respect to δ .

APPENDIX B

Let $P(\delta_l, q)$ be the probability distribution for the linear density fluctuation, δ_l , at a fixed Lagrangian distance, q , from the center of an object and let $P(\delta, r)$ be the probability distribution for the actual density fluctuation, δ , at a fixed Eulerian distance, r , from the center of the same object. We shall show that the following relationship holds:

$$\int_{\delta_0}^{\infty} P(\delta, r) d\delta = \int_{\delta_l(\delta_0)}^{\infty} P(\delta_l, q = r(1 + \delta_0)^{\frac{1}{3}}) d\delta_l \quad (\text{B1})$$

from which expressions (9) and (26) immediately follow.

If δ_l takes the value $\delta_l(\delta_0)$ at Lagrangian radii $r(1 + \delta_0)^{\frac{1}{3}}$, it is clear that, by construction, δ must take the value δ_0 at Eulerian radii, r . Now, if at Eulerian radii r , δ takes a value, δ' , larger than δ_0 , its corresponding Lagrangian radii, q' , must satisfy:

$$q' = r(1 + \delta')^{\frac{1}{3}} > r(1 + \delta_0)^{\frac{1}{3}} = q$$

and the value of δ_l at q' , $\delta'_l = \delta_l(\delta')$, must be larger than $\delta_l(\delta_0)$. But, if the linear profile is monotonically decreasing the value of the linear density fluctuation at q , δ_l , must be larger than the value at q' , δ'_l , which is, ex hypothesi, larger than $\delta_l(\delta_0)$. So, whenever δ is larger than δ_0 at r , δ_l is larger than $\delta_l(\delta_0)$ at $q = r(1 + \delta_0)^{\frac{1}{3}}$, hence, (B1) follows. Note that, if $P(\delta_l, q)$ vanishes for $\delta_l > \delta_{vir}$, the upper limit in the right hand side of (B1) may be set equal to δ_{vir} .

REFERENCES

- Avila-Reese, V., Firmani, C. & Hernandez, X. 1998, *ApJ*, 505, 37
 Ascasibar, Y., Yepes, G., Gottloeber, S. & Mueller, V. 2004, *MNRAS*, 352, 1109
 Bajtlik S., Duncan R. C., Ostriker J. P., 1988, *ApJ*, 327, 570
 Bardeen, J. M., Bond, J. R., Kaiser, N. & Szalay, A. S. 1986, *ApJ*, 304, 15 (BBKS)
 Barkana R., 2004, *MNRAS*, 347, 59
 Bernardeau, F. 1994, *ApJ*, 427, 51
 Bertschinger, E. 1985, *ApJS*, 58, 39
 Brainerd, T.G., 2004, *astro-ph/0409381*
 Conroy, C., Newman, J. A., Davis, M., Coil, A. L., Yan, R., Cooper, M. C., Gerke, B. F., Faber, S. M., & Koo, D. C., 2004, *astro-ph/0409305*
 Fillmore, J. A. & Goldreich, P. 1984, *ApJ*, 281, 1
 Gunn, J. E. & Gott, J. R. 1972, *ApJ*, 176, 1
 Gunn J. E., 1977, *ApJ*, 218, 592
 Gurevich, A. V. & Zybin, K. P. 1988, *ZHETF*, 94, 3
 Guzik, J., & Seljak, U., 2002, *MNRAS*, 335, 311
 Hoekstra, H., Yee, H. K. C., Gladders, M. D., 2004, *ApJ*, 606, 67
 Hiotelis, N. 2002, *A*, 382, 84
 Hoffman Y., Shaham J., 1985, *ApJ*, 297, 16
 Jenkins A., Frenk C. S., White S. D. M., Colberg J. M., Cole S., Evrard A. E., Couchman H. M. P., Yoshida N., 2001, *MNRAS*, 321, 372
 Kravtsov, A.V., Klypin, A.A., & Khokhlov, A.M., 1997, *ApJS*, 111, 73
 Lilje, P.B., Yahil, A. & Jones, B.J.T. 1986, *ApJ*, 307, L91
 Lokas E. L., 2000, *MNRAS*, 311, 423
 Lokas, E. L. & Hoffman, Y. 2000, *ApJ*, 542, L139
 Nusser, A. 2001, *MNRAS*, 325, 1397
 Padmanabhan T., 1996, *MNRAS*, 278, L29
 Patiri S., Betancort-Rijo J. E. & Prada F. 2004, *astro-ph/0407513*
 Prada, F., Vitvitska, M., Klypin, A., Holtzman, J. A., Schlegel, D. J., Grebel, E. K., Rix, H.-W., Brinkmann, J., McKay, T. A., & Csabai, I., 2003, *ApJ*, 598, 260
 Prada F., Klypin A. A., Simmoneau E., Betancort-Rijo J., Patiri S. G., Gottlöber S., Sanchez-Conde M. A., 2005 *astro-ph/0506432*
 Ryden, B. S. & Gunn, J. E. 1987, *ApJ*, 318, 15
 Sheldon, E. S., et al., 2004, *AJ*, 127, 2544
 Sheth, R. K. & Tormen, G. 2002, *MNRAS*, 329, 61
 Sikivie, P., Tkachev, I. I. & Wang Y. 1997, *Phys. Rev. D*, 56(4), 1863
 Smith, D. R., Bernstein, G. M., Fischer, P., & Jarvis, M., 2001, *ApJ*, 551, 643
 Subramanian K., Cen R., Ostriker J. P., 2000, *ApJ*, 538, 528
 White, S. D. M. & Zaritsky, D. 1992, *ApJ*, 394, 1
 Zaritsky, D. & White, S. D. M. 1994, *ApJ*, 435, 599
 Zaritsky, D., Smith, R., Frenk, C., & White, S. D. M. 1997, *ApJ*, 478, 39